

Dispersion of Nanoclays with Poly(ethylene terephthalate) by Melt Blending and Solid State Polymerization

Sung-Gi Kim, Elizabeth A. Lofgren, Saleh A. Jabarin

Department of Chemical and Environmental Engineering and Polymer Institute, University of Toledo, Toledo, Ohio 43606-3390

Correspondence to: S. A. Jabarin (E-mail: saleh.jabarin@utoledo.edu)

ABSTRACT: Melt intercalation of clay with poly(ethylene terephthalate; PET) was investigated in terms of PET chain mobilities, natures of clay modifiers, their affinities with PET, and nanocomposite solid state polymerization (SSP). Twin screw extrusion was used to melt blend PET resins with intrinsic viscosities of 0.48, 0.63, and 0.74 dL/g with organically modified Cloisite 10A, 15A, and 30B montmorillonite clays. Clay addition caused significant molecular weight reductions in the extruded PET nanocomposites. Rates of SSP decreased and crystallization rates increased in the presence of clay particles. Cloisite 15A blends showed no basal spacing changes, whereas the basal spacings of Cloisite 10A and Cloisite 30B nanocomposites increased after melt extrusion, indicating the presence of intercalated nanostructures. After SSP these nanocomposites also exhibited new lower angle X-ray diffraction peaks, indicating further expansion of their basal spacings. Greatest changes were seen for nanocomposites prepared from the lowest molecular weight PET and Cloisite 30B, indicating its greater affinity with PET and that shorter more mobile PET chains were better able to enter its galleries and increase basal spacing. © 2012 Wiley Periodicals, Inc. *J. Appl. Polym. Sci.* 000: 000–000, 2012

KEYWORDS: poly(ethylene terephthalate); clay; nanocomposites; melt intercalation; thermal stability; XRD

Received 15 December 2011; accepted 27 March 2012; published online

DOI: 10.1002/app.37796

INTRODUCTION

Poly(ethylene terephthalate; PET) is a semicrystalline polymer, with applications that include beverage bottles, textiles, and films.¹ Incorporation of exfoliated clay nanoparticles into PET can decrease oxygen permeability through food packaging, increase flame resistance of textiles, and increase tensile modulus of injection molded parts. Traditional fillers used to improve properties and reduce costs have limited applications because of phase separation, particle agglomeration, and heterogeneous distributions in the polymer matrix.² These problems can be reduced through optimized dispersion of the nanoclay, which may be achieved by maintaining small clay particle sizes as well as through clay surface treatments to create an affinity between the clay and the polymer.

Polymer nanocomposites may contain nanometer scale clay particles with high aspect ratios. The clays are composed of layers and enhancement of nanocomposite properties can vary according to their distribution in a polymer matrix.^{3–6} Tactoid structures are obtained when there is poor affinity with the polymer and the interlayer spaces of the clay do not expand. In the case of intercalated structures there is some affinity between the polymer and the clay, creating low levels of clay interlayer

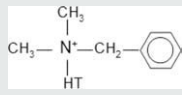
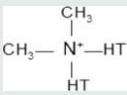
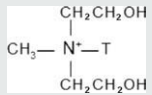
expansion and well-ordered stacked multilayer structures. In the case of exfoliated structures, the clay layers have lost their registry and are well separated into single platelets within a continuous polymer matrix. This form is preferred and occurs if there is very good affinity between the polymer and clay.

Exfoliated structures give the greatest property improvements and exhibit the highest levels of clay dispersity and interfacial polymer interactions. The appropriate hydrophobicity of clay and compatibility between organically modified clay and polymer are critical factors in nanocomposite formation.⁷ Large interlayer spacing in the clay, as well as the likelihood for an interaction to occur between the clay and polymer, also must be considered in order to develop exfoliated nanostructures.

Polymer clay-nanocomposites can be prepared using solution mixing, *in situ* polymerization methods, or melt blending.^{7–9} In the case of melt blending, polymer and clay are combined in an extruder under shear and above the softening temperature of the polymer. This method has several advantages over other methods, since no environmentally harmful solvents are required and nanocomposite residence times at high temperatures are shorter than in the case of *in situ* polymerization. In

© 2012 Wiley Periodicals, Inc.

Table I. Comparison of the Three Clays in Terms of Potential Expansion of Basal Spacing²¹

Factors	Cloisite 10A	Cloisite 15A	Cloisite 30B
Modifier structure			
Basal spacing	19.2 Å	31.5 Å	18.5 Å
Compatibility ^a	+	0	++
Modifier concentration	125 mequiv/100 g	125 mequiv/100 g	90 mequiv/100 g
Interaction force ^a	0	0	+
Hydrophobicity	Low	High	Very low

^a+, positive effect; -, negative effect.

HT represents hydrogenated tallow (~ 65% C18; ~ 30% C16; ~ 5% C14); T indicates tallow (~ 65% C18; ~ 30% C16; ~ 5% C14).

addition, commercial scale production can be achieved with current industrial and processing techniques.

Natural montmorillonite is a layered hydrophilic material. A cation exchange reaction can be used to replace sodium, calcium, or potassium naturally present in the clay with a cationic surfactant such as primary, secondary, tertiary, and quaternary alkyl ammonium or alkylphosphonium cations. When the clay surface is thus modified, its surface energy is reduced and its properties become more organophilic than those exhibited by natural clay giving it more affinity with a polymer. Basal spacing of the organically modified clay is expanded, due to the bulkiness of alkyl ammonium or alkylphosphonium cations. These cations may also provide functional groups to react with the polymer or initiate polymerization of monomers.^{10–13}

Natural and synthetic clays can act as catalysts¹⁴ whose activities can be affected by surface areas, amounts of agglomeration, clay morphology, and temperature. Sposito et al.¹⁵ investigated degradation mechanisms of organically modified clay and found that thermal decompositions of the modifiers were initiated in the portions with the smallest bond dissociation energies and that the modified clays can still be used to form nanocomposites, even after initiation of thermal degradation.

The most common techniques used to elucidate nanocomposite structures are wide angle x-ray diffraction (XRD) and transmission electron microscopy (TEM), which is used to verify exfoliation in the absence of XRD peaks. The presence of an XRD peak indicates that complete exfoliation has not occurred.

Previous researchers^{16–19} have attempted to achieve optimized dispersions of various clays through melt mixing in a PET matrix. The current work combines melt blending with solid state polymerization (SSP) in order to create better dispersions of the clays. For this purpose we have used montmorillonite clays with three different organic modifications. As a result of their modifications, these clays should exhibit different affinities with PET and different basal spacings. In addition to clay differences, PET resins of different initial molecular weight or intrinsic viscosity (I.V.) values have been utilized, in order to determine if the greater mobility of lower molecular weight PET could achieve better penetration of the clay basal spacing. This research

includes x-ray diffraction examination of changes in the basal spacings of nanostructures attained through melt mixing, the reasons for molecular weight reductions after extrusion (through end group concentration analysis), the effects of solid state polymerization on the nanostructures and their basal spacings, as well as the thermal characteristics of the nanocomposites.

This study comprises Part I of this work and is directed toward investigations concerning melt intercalation (blending) of clay with PET. Special attention has been given to the thermal stability of PET during melt blending. Part II of the research continues these nanocomposite investigations through the use of *in situ* polymerization.²⁰

EXPERIMENTAL

Materials

Voridian Aqua WA314 PET resin, commercially SSP to an intrinsic viscosity (IV) of 0.74 dL/g, was melt blended with the clay using a twin screw extruder. Additional blending was done using non-SSP PET resins with lower initial IV values of 0.48 dL/g and 0.63 dL/g, produced and provided by SK Chemicals. The lower IV resins were used to evaluate the effects of initial PET molecular weight on melt intercalation. Cloisite 10A, 15A, and 30B organically modified montmorillonite clays were obtained from Southern Clay Products, and used to prepare the nanocomposites without further chemical treatment. Significant characteristics of each of these clays are summarized in Table I.²¹ Cloisite 10A includes a benzene ring, which indicates the possibility of its compatibility with the PET benzene ring structure. The tallow modified Cloisite 15A has the highest level of basal spacing; therefore, the PET chains would be expected to more easily penetrate its interlayer spacing. Cloisite 30B has two hydroxyl groups in the modifier, which suggest the possibility of compatibility with the hydroxyl groups of PET as well as interactions with its carboxyl groups. In addition to the existence of hydroxyl groups, Cloisite 30B exhibits the smallest cation exchange capacity (CEC) among three clays. As a result, separation of Cloisite 30B platelets is expected to be less difficult than for either of the other two clays.

Twin Screw Extrusion

A Werner & Pfleiderer ZSF-30 co-rotating twin screw extruder equipped with a vacuum pump was used to compound the PET resins with each of the various clays at compositions from 0 to 5% wt./wt. clay {(weight of each modified clay/total weight of nanocomposite)100}. To achieve homogeneous dispersions of the clay particles in the PET matrix, melt mixing was performed at 200 rpm, with zone 1 (nearest the hopper) at 200°C, and mixing zones 2–4 and the extruder die at 275°C. Extruder throughput was 10 Kg/h. Before extrusion, the PET resins were dried in a Conair desiccant dryer at 140°C overnight and the clays were vacuum dried at 120°C overnight to remove free water. Dry blend mixing of the PET and clay was performed for 3 min in a sealed metal container, immediately before loading the mixture into the hopper of the extruder. Nanocomposite strands exiting the extruder die were quenched as they passed through a water bath and pelletized. The residence time in the extruder (3–5 min) was measured as the interval between when the mixture entered the extruder barrel and the time the extrudate exited the die.

Solid State Polymerization

To prevent the pellets from sticking, amorphous samples were precrystallized at 150°C for 2 h before SSP. A laboratory scale Buhler reactor, with a 1000 g sample capacity, was used to perform SSP. The cylindrical, stainless steel reactor was designed to pass preheated nitrogen (N₂) through the pellet bed during SSP to evenly distribute heat throughout the sample chamber and remove volatile products from the pellets. Preheating the pellets from room temperature to the SSP temperature required 1.5 h. Reaction times were taken after the resin reached 210°C at the nitrogen flow rate of 2000 L/h and 0.3 bar pressure.

Intrinsic Viscosity

Intrinsic viscosities (IV) of the samples were measured through the conversion of melt viscosity into intrinsic viscosity. Melt viscosities were measured at a temperature of 280°C and shear rate of 10 rad/s (equivalent to zero shear viscosity), using a Rheometrics viscoelastic tester with parallel-parallel plate geometry. A calibration curve was obtained from a plot of the relationship between intrinsic viscosity, determined in a 60/40 phenol/tetrachloroethane solvent system and melt viscosity values. Three PET resins and four nanocomposite samples, each containing 3 wt % clay, were used to obtain the correlation given in eq. (1).

$$IV = 0.126 * \ln(\text{melt viscosity [Pa s] at 10 rad/s}) - 0.040 \quad (1)$$

Thermal Stability

A rheometrics viscoelastic tester with parallel plate geometry was used to measure the melt viscosity as a function of time. Measurements were performed under nitrogen or air at 280°C and 10 rad/s for 20 min. Before melt viscosity measurements, all samples were vacuum dried at 140°C overnight. To compare relative degrees of degradation in the melted state, melt viscosities were normalized by dividing each value by its maximum melt viscosity.

Carboxyl and Hydroxyl End Group Concentration Using FTIR

Carboxyl end group concentrations of PET nanocomposites were determined using a Fourier Transform Infrared (FTIR) technique that has previously been described^{22,23} and modified by Kim et al.²⁴ Current study employed the method variations developed by Kim et al.²⁴ that utilize peak intensities at specific wave numbers, rather than peak areas for calculations. A calibration curve was used to establish the exact relationship between normalized intensity differences obtained with FTIR (ΔN_{COOH}) and carboxyl end group contents measured according to the titration method described by Jabarin and Lofgren.²⁵

In preparation for FTIR measurements, all the crystalline samples were vacuum dried at 140°C, while the amorphous pellets were dried at 80°C. The cylindrical pellets were then compression molded between polished metal dies to obtain thin film samples, maintained under dry conditions. Thicknesses of less than 0.3 mm were found to give optimum reproducibility. As previously described,²⁴ FTIR measurements were performed in the transmission mode, under a nitrogen atmosphere. Normalization of absorption spectrum intensity (N_{COOH}) was done after the intensity at 3714 cm⁻¹ was set at zero to eliminate thickness effects. Next, the intensity at 3268 cm⁻¹ was normalized with the intensity at 3995 cm⁻¹ for the carboxyl end group concentration. Deuterated samples were prepared with the reaction of deuterium oxide and sample at 50°C for more than 48 h to provide zero levels of end groups. All the samples were dried before deuteration. Equation (2) was used to calculate normalized intensity difference (ΔN_{COOH}) values for each sample.

$$\Delta N_{\text{COOH}} = N_{\text{COOH}} - N_{\text{COOH-d}} = \left[\frac{I_{3268\text{cm}^{-1}} - I_{3714\text{cm}^{-1}}}{I_{3995\text{cm}^{-1}} - I_{3714\text{cm}^{-1}}} \right]_{\text{sample}} - \left[\frac{I_{3268\text{cm}^{-1}} - I_{3714\text{cm}^{-1}}}{I_{3995\text{cm}^{-1}} - I_{3714\text{cm}^{-1}}} \right]_{\text{deuterated-sample}} \quad (2)$$

According to the method of Kim et al.,²⁴ a calibration curve was obtained from normalized FTIR intensity differences and carboxyl end group contents measured by titration. The calibration yielded the following relationship: COOH (titration) = 20.659* ΔN_{COOH} . Each reported value represents the average of 4–5 individual sample measurements.

Hydroxyl end groups were measured in the same manner as the carboxyl end groups; however, the intensity at 3268 cm⁻¹ was replaced by intensity at 3545 cm⁻¹, giving the relationship: OH = 26.0* ΔN_{OH} .

DSC Measurement

A Perkin–Elmer DSC-7, differential scanning calorimeter, was used to monitor glass transition (T_g), crystallization from the glassy state (T_{c1}), and melting (T_m) temperatures of samples heated at rates of 10°C/min. Temperatures of crystallization from the melt (T_{c2}) were measured at cooling rates of 5°C/min. All samples were evaluated under a nitrogen atmosphere.

Basal Spacing Measurement by Wide Angle X-Ray Diffraction

The basal spacings of the nanocomposites and clays were determined with wide angle x-ray diffraction. All samples were

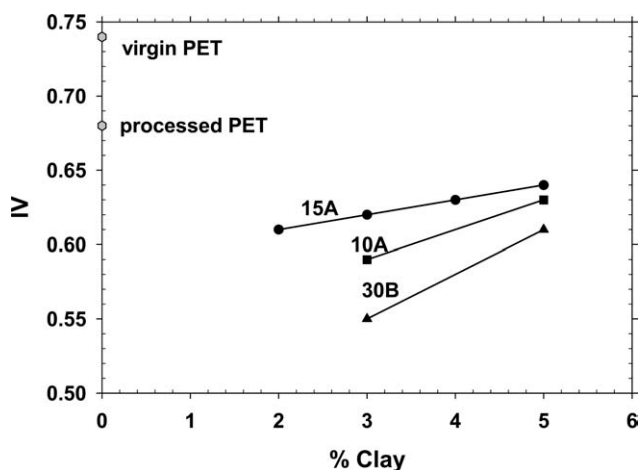


Figure 1. Nanocomposite IV values are shown after extrusion of IV 0.74 dL/g PET with Cloisite 15A in amounts of 2, 3, 4, and 5 wt %. Cloisite 10A and 30B nanocomposites are shown after extrusion with the same IV PET at concentrations of 3 and 5 wt %. Initial PET IV is shown as virgin PET and unmodified extruded material as processed PET.

ground into fine powder in preparation for measurement. A Scintag Inc XDS 2000 powder diffractometer, with a 0.154 nm radiation source, was used to measure the interlayer spacing of the samples. A liquid nitrogen cooled germanium solid state detector was used to capture the scattered X-ray beam at a scan speed of 0.2°/min, and in the range of $2\theta = 1.6^{\circ}$ – 7° .

Basal spacing calculations were done according to the Bragg equation,²⁶ where θ is inversely proportional to basal spacing as shown in eq. (3). For this equation, n = integer, λ = wavelength, d = the separation of atomic plane (basal spacing or d -spacing in the clay), and θ = the angle between direction of travel of the wave and the atomic plane.

$$n\lambda = 2d \sin \theta \text{ (Bragg equation)} \quad (3)$$

RESULTS AND DISCUSSION

Three different organically modified clays were used to evaluate the various effects of melt mixing with PET. Important characteristics of these clays are summarized in Table I. As can be seen the Cloisite 10A has a benzene ring structure and a lower range of hydrophobicity, Cloisite 15A has the largest basal spacing as well as high hydrophobicity, while the Cloisite 30B clay contains hydroxyl groups and has very low hydrophobicity. These three materials were chosen for evaluation to determine which chemical modifications would enhance the affinity of clay with PET and what factors have the greatest effects on resultant nanostructures.

The first set of nanocomposites was prepared by melt-blending various concentrations of each of the three clays with 0.74 dL/g IV PET. Addition of the clay materials was found to cause a much larger decrease in extrudate IV than was observed for equivalent extruded unblended PET. Figure 1 shows IV values measured for virgin and processed PET as well as each of the extruded PET/clay blends. An IV decrease of 0.06 dL/g is observed in the case of unblended PET, whereas the presence of

only 2% Cloisite 15A clay causes an IV decrease of 0.13 dL/g. The presence of the other two clays caused even greater losses in IV, with the Cloisite 30B nanocomposites showing the greatest decreases in IV.

Results given in Figure 1 also indicate that increasing levels of clay in the extruded samples cause slight increases of their IV values. Matayabas Jr. and Turner⁹ reported that the addition of clay caused a large IV decrease and that larger decreases were observed for samples containing higher levels of clay. Our results, however, show that melt viscosities increase with the addition of increased amounts of clay. These variations in blend properties may be caused by the use of different organic clays. They used Clayton APA, whereas current study utilizes Cloisite materials.

Xie et al.²⁷ investigated thermal degradation of organically treated montmorillonite, and suggested four decomposition regions with respect to exposure temperature in a thermal gravimetric analyzer (TGA). The free water was released in the region below 200°C, organic substances evolved in the region between 200°C and 500°C, structural water was released in the region between 500°C and 800°C, and organic carbon reacted in the region between 800°C and 1000°C. They reported that the onset temperature of thermal degradation did not mean that the clay could not be used to form nanocomposites at that temperature. Davis et al.¹⁸ stated that the natures of organic modifiers in montmorillonite can affect its thermal stability, dispersion, and delamination in PET nanocomposites. The decomposition mechanisms and temperatures of organic clays used in this research, therefore, could be different, according to the chain lengths and the chemical groups of the clay modifiers.

Another characteristic of PET nanocomposites is their non-Newtonian behaviors in the relationships between their melt viscosities and shear rates, even in the regions of low shear rates. PET shows Newtonian behavior in the low shear rate region, so that melt viscosity at 10/s can be used to express the molecular weight in terms of PET solution viscosity. As can be seen in Figure 2 increased amounts of Cloisite 15A clay cause

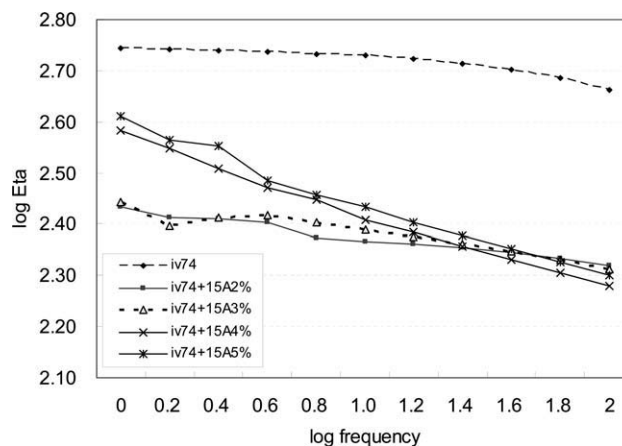


Figure 2. Melt viscosity changes are shown as functions of low shear rates, for unmodified PET and Cloisite 15A nanomaterials. The virgin PET had an initial IV of 0.74 dL/g and the Cloisite 15A clay was compounded at concentrations of 2, 3, 4, and 5 wt %.

non-Newtonian behavior in melt viscosity of the nanocomposites. Nanocomposites containing larger amounts of clay (4, 5 wt %) show pseudo-solid-like behavior, exhibiting an almost linear relationship between shear viscosity and shear rate. Samples containing smaller amounts of clay (2, 3 wt %) show shear thinning behavior, illustrated as a gradual decrease of shear viscosity at high shear rate due to orientation. Similar trends were observed in all three clay nanocomposites. Krishnamoorti and others^{12,28} explained these phenomena in terms of yield stress. Some values of yield stress are needed to move the system in the cases of higher contents of clay, while almost zero yield stress is required at lower contents of clay. Divergence of shear viscosity at low shear rates is related to pseudo-solid-like behavior at higher contents of clay in nanocomposites. At higher shear rates, the parallel orientation of clay layers or tactoids in the flow direction causes the melt viscosity of the nanocomposites to undergo shear thinning.

Since reported IV results were obtained in this research by conversion from melt viscosity at 10/s shear rate to solution viscosity, it is possible that nanocomposite IV values could be slightly overestimated in the cases of blends containing 4 and 5 wt % clays. The correlation curve, however, was obtained with three pure PET samples and five nanocomposites, each containing 3 wt % clay.

In order to examine the effects of PET molecular weight on degree of intercalation into the clay galleries, the three clays (Cloisite 10A, 15A, and 30B) were compounded with two additional lower IV samples of 0.63 and 0.48 dL/g. These experiments were performed to explore the concept that shorter molecules of PET would be able to penetrate the interlayer spaces of the clays more easily than the longer, higher IV molecules. As with the higher IV PET, addition of 3 wt % clay caused significant losses in the IV values of the extruded nanocomposites. Figure 3 compares the initial virgin PET IV values with those obtained for 3% nanocomposites prepared with each of the clays. As can be seen, the higher IV PET nanocomposites exhibited in the greatest IV drops. The blends containing 15A clay showed the smallest decreases in IV and those containing 30B clay showed the greatest decreases, regardless of initial PET IV. This greater level of IV decrease may have occurred because the Cloisite 30B clay has two hydroxyl groups in its modifier. Introduction of these polar hydroxyl groups could have caused enhanced interaction with polar groups such as moisture in the air and thus accelerated further hydrolytic and/or oxidative degradation of the nanocomposites at the 275°C extrusion/processing temperature.

Possible mechanisms involved in the decreased IV or molecular weight values of extruded nanocomposites, have been evaluated in terms of the relative influences of several degradation processes. The observed reductions could have occurred as a result of hydrolytic, thermal, and/or oxidative degradation.^{1,29–31} These modes of degradation are known to occur in the region from 260 to 300°C, the temperature range required for PET melt processing or polymerization. Although all three types of degradations can cause molecular weight reductions, each type of degradation proceeds in a different way. Hydrolytic degradation is the most rapid form of degradation among the three mecha-

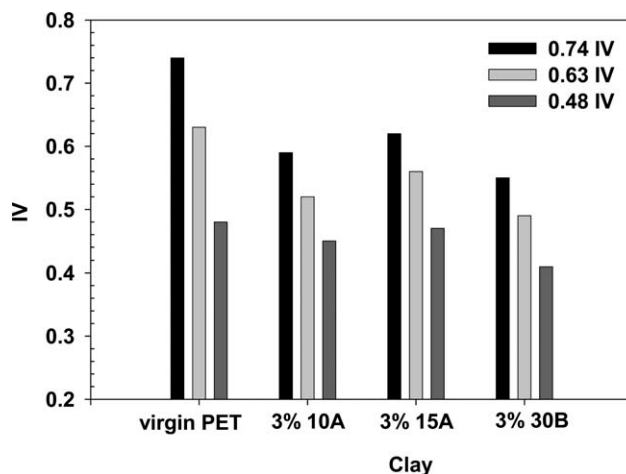


Figure 3. IV values of 0.74, 0.63, and 0.48 dL/g IV PET are shown before extrusion in comparison to nanocomposite values after extrusion of the three PET materials, each compounded with 3 wt % concentrations of the Cloisite 10A, 15A, and 30B clays.

nisms. It is known to increase the carboxyl and hydroxyl end group concentrations as a result of the reverse reaction of esterification.¹ Hydrolysis can be affected by moisture exposure (such as from inadequate drying), temperature, acidity, and types of catalysts.^{29–33}

Thermal degradation can follow complex degradation schemes. Previous researchers^{34–36} have suggested several mechanisms for degradation; however, no single unique mechanism seems to exist. Common points in each degradation scheme include the formation of vinyl ester groups, acetaldehyde, and carboxyl end groups. The results of all these higher temperature mechanisms are molecular weight reductions, even though reactions are said to occur at chain ends or at ester linkages.

It is reported that oxygen accelerates the thermal degradation reaction so that discoloration, branched chains, gelation, and formation of several gaseous products can be detected more often than when PET is exposed to high temperatures in the absence of oxygen.^{29,31} It is believed that oxidative degradation of PET includes a free radical mechanism, which can increase the reaction rate.

Thermal stability investigations were conducted with a parallel plate rheometer at 280°C, under nitrogen and air in order to elucidate the main sample degradation mechanisms (hydrolytic, thermal, and oxidative) responsible for the observed decreases. The effects of moisture, heat, and oxygen were evaluated separately on PET and each organically modified nanocomposite. Figure 4(a,b) shows normalized melt viscosity changes recorded for pure PET and the 3 wt % nanocomposites under respective atmospheres of nitrogen (N₂) and air.

Figure 4(a) shows the effects of thermal degradation on the melt viscosity of 0.74 IV PET and the various nanocomposites with IV values in the range of 0.60 dL/g. In this case, oxygen was eliminated by the nitrogen flow in the rheometer chamber and moisture was excluded by both vacuum drying of samples and nitrogen flow in the rheometer. The melt viscosity of PET

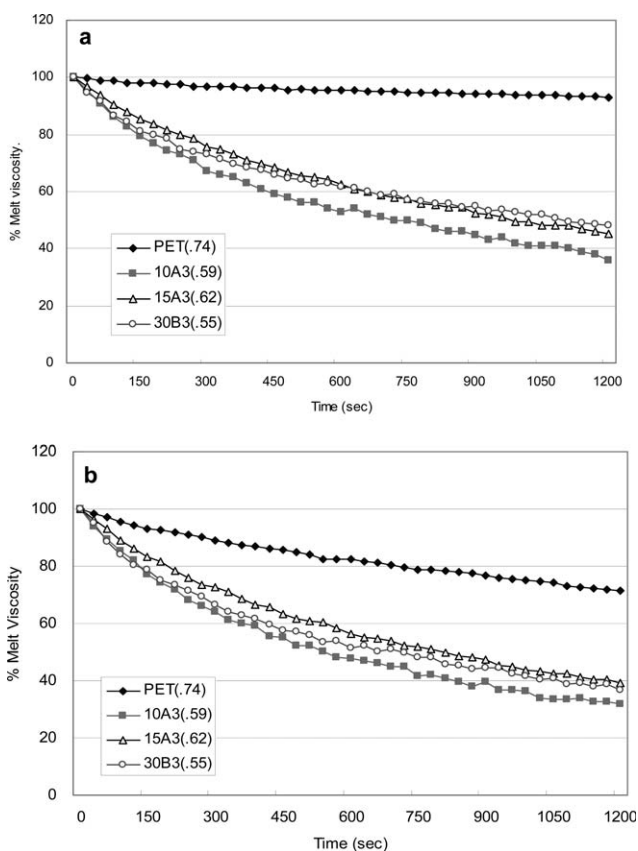


Figure 4. Thermal stabilities of PET and its nanocomposites (with initial IV values near 0.60 dL/g) are shown in terms of changing % melt viscosity values. Changes are observed for samples held at 280°C for 20 min. Clay amounts are fixed at 3 wt % of the Cloisite 10A, 15A, and 30B materials and the sample initial IV values are shown in parenthesis. The upper (a) figure gives results obtained for samples heated under a nitrogen atmosphere, whereas the lower (b) figure gives similar results obtained under an air atmosphere.

remained at an almost constant value for 20 min. All PET nanocomposites; however, showed drastic declines of their melt viscosities. Thermal stabilities of the nanocomposites held at 280°C under air [Figure 4(b)] show trends similar to those of the nanocomposites heated under nitrogen; however, the melt viscosity changes decreased by an additional 10%. The melt viscosity of PET was found to decrease by 30% during heating under air, confirming that its rate of degradation is accelerated in the presence of oxygen. The melt viscosity drop of PET heated under air was approximately half that of the nanocomposites heated under nitrogen.

Changes in end group concentrations can be used to indicate modes of polymer degradation. The initial carboxyl end group concentration of the commercially solid stated 0.74 IV PET was found to be 10 mmol/kg PET, whereas the hydroxyl end group concentration was 46 mmol/kg PET. After thermal degradation of the 0.74 IV resin in nitrogen or air [shown in Figure 4(a,b)] these end group concentrations changed. The carboxyl end group value measured after heating under nitrogen increased from 10 to 18 mmol/kg PET, whereas the hydroxyl end group

value slightly decreased from 46 to 44 mmol/kg PET. These changes can be explained by thermal degradation effects on PET. Oxidative thermal degradation effects were demonstrated in a similar experiment performed under air. The carboxyl end group value of 0.74 IV PET, heated at 280°C for 20 min under air, increased from 10 to 50 mmol/kg PET. The hydroxyl end group value also increased from 46 to 62 mmol/kg PET. It can be seen that significantly more end groups are found in the PET, if air is present during otherwise equivalent thermal exposure conditions. With these results, we can distinguish the occurrence of thermal degradation from that of oxidative thermal degradation.

McMahon et al.³⁷ reported that the hydrolysis rate is 10,000 times faster than the thermal degradation rate, and 5000 times faster than oxidative thermal degradation at the same temperature. Thermal stability of PET in the melt state is affected greatly by the presence of various metal compounds,³⁸ and carboxyl end groups can be increased even in the solid state according to drying temperature.

Carboxyl and hydroxyl end group values were determined for various clay blends compounded using the PET resin with an initial IV of 0.74 dL/g. Figure 5 gives an overview of these results. As can be seen, the compounded materials containing Cloisite 10A and Cloisite 15A exhibit an average carboxyl end group concentration of 19 mmol/kg PET. This is a 9 mmol/kg PET increase in carboxyl concentration in comparison to that of unblended PET.

Hydroxyl end group values of nanocomposites containing Cloisite 10A and Cloisite 15A increased from that of the 0.74 IV PET by an average of 14 mmol/kg PET. When we compare the increases of both end group concentrations ($-\text{COOH} = 9$ mmol/kg PET and $-\text{OH} = 14$ mmol/kg PET), we can conclude that the main reason for molecular weight reduction is hydrolysis. If thermal degradation had been the main reason, only-COOH

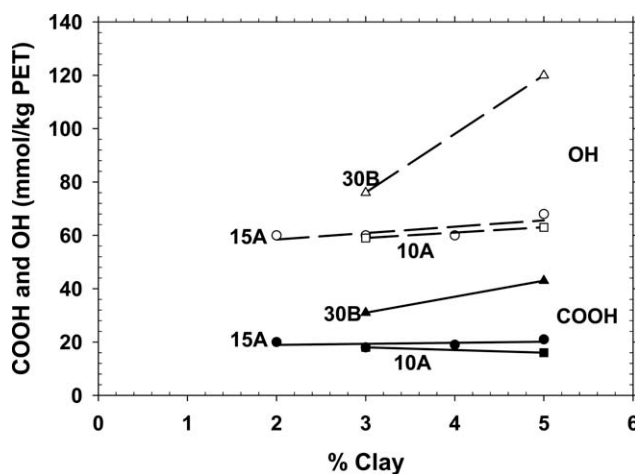


Figure 5. Carboxyl end group concentrations (filled symbols) and hydroxyl end group concentrations (open symbols) are shown for nanocomposites extruded with IV 0.74 dL/g PET. Cloisite 15A clay was compounded at concentrations of 2, 3, 4, and 5 wt %, whereas Cloisite 10A and 30B nanocomposites are shown at concentrations of 3 and 5 wt %.

concentrations should have increased. If oxidative thermal degradation had been the main reason, then the $-\text{COOH}$ values should be much higher (more than 2 times) than 19 mmol/kg PET. The moisture absorption rate of the nanocomposite seems to be faster than that of the unblended PET, because of the presence of the clay component, even though all samples were vacuum dried. The clay particles have extremely large surface areas and this may accelerate the moisture absorption rate during melt mixing in the hopper of the extruder.

Carboxyl and hydroxyl end group values of Cloisite 30B clay compounded with 0.74 IV PET are much higher than measured for the other nanocomposites. This appears to be related to acceleration of degradation due to the hydroxyl groups of the modifier in the Cloisite 30B.

These experimental results can be summarized in the following manner. (a) IV reduction of nanocomposites is more than twice as great as that of pure PET, even when the drying and extrusion conditions are equivalent. (b) The presence of clay increases the rates of degradation of the nanocomposites and causes severe molecular weight reductions. (c) Although several degradation mechanisms could be involved in molecular weight reductions of the nanocomposites, the relative increases of carboxyl and hydroxyl end groups indicate that hydrolysis is the main reason for their degradation during melt mixing.

To examine the effects of organically modified clay on the thermal characteristics of the various nanocomposites, the glass transition temperature (T_g), crystallization temperature when heating from room temperature (T_{c1}), melting temperature (T_m), and crystallization temperature when cooling from 300°C (T_{c2}) were measured using dynamic DSC. The T_g values of all the nanocomposites (ranging from 75 to 77°C) decreased about 1–3°C from those of the unblended PET resins used in their preparation. Results obtained for the three unblended PET resins of different IV showed similar reductions in T_g related to reduced resin IV, indicating that the nanocomposite trend is related to molecular weight reduction after extrusion. Melting peak temperatures of the nanocomposites ranged from 246 to 247°C. These values also did not show major changes from those of unblended PET.

Although no significant differences were recorded for glass transition and melting temperatures; melt mixing of PET with clay drastically changed the observed crystallization behaviors of the nanocomposites. Figure 6(a) gives a comparison of crystallization peak temperatures (T_{c1}), obtained while heating quenched amorphous PET and the various nanocomposites from the glassy state. The presence of clay in the nanocomposites results in a 35°C decrease in T_{c1} . This indicates much faster rates of crystallization than observed for the unblended PET resins.

The previously described samples were also cooled from the melt to further examine their thermal behaviors. Figure 6(b) shows peak crystallization temperatures (T_{c2}) recorded at a cooling rate of 5°C/min. As can be seen, these T_{c2} values increased by an average value of 25°C indicating faster rates of crystallization for nanocomposites in comparison to pure PET. Crystallization rates are strongly sensitive to the presence of nucleating agents, which may increase these rates more signifi-

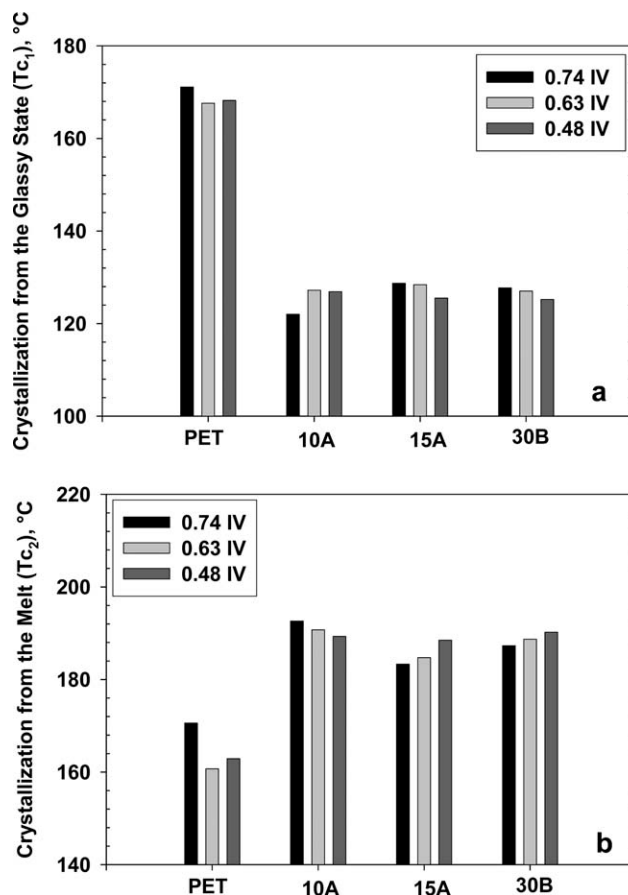


Figure 6. Peak crystallization temperatures are shown for three different IV PET materials and for their nanocomposites, compounded with 3 wt % Cloisite 10A, 15A, and 30B. The upper (a) figure gives (T_{c1}) results for samples reheated from the glassy state at 10°C/min after being quenched from the melt. The lower (b) figure gives (T_{c2}) crystallization temperatures recorded for samples cooled from the 300°C melt at a rate of 5°C/min.

cantly than reductions in polymer molecular weight. Ebengou³⁹ reported that the nucleation process governs the crystallization kinetics. Heterogeneous nucleation occurs in polymer systems and impurities can act as active nucleation sites. The large changes in T_{c1} and T_{c2} in the presence of nanocomposites show the strong dependency of crystallization rate on the clay particles acting as nuclei. Although crystallization rates can be increased as a result of polymer IV reductions, these effects were negligible in comparison to the much greater nucleating effects of the clay particles.

Solid state polymerization of the organically modified nanocomposites was thought to possibly enhance dispersion of the clays. For these investigations, PET resin with an IV of 0.63 dL/g was solid state polymerized at 220°C for 15 h with a N_2 flow rate of 700 L/h and 0.3 bar N_2 pressure. This sample achieved a final IV of 1.00 dL/g, with an IV increase of 0.37 dL/g. Equivalent conditions were used to SSP the various nanocomposites. Their IV values before and after SSP are shown in Figure 7. Differences in these values indicate their relative SSP rates. Addition of the clays was found to make their SSP rates much

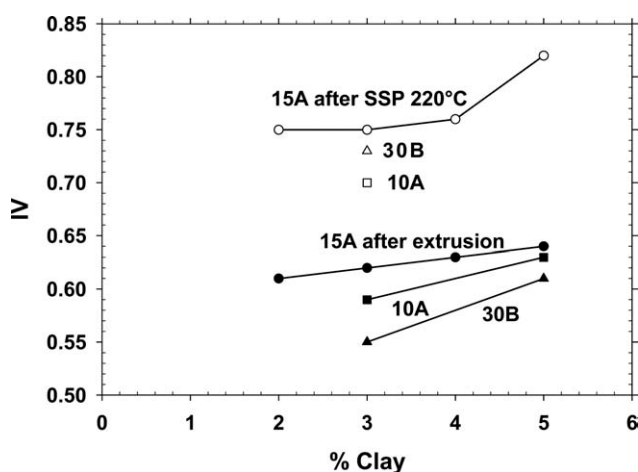


Figure 7. Nanocomposite IV values are shown after extrusion (filled symbols) and after solid state polymerization (open symbols) at 220°C for 15 h. Nanocomposites were prepared from 0.74 dL/g IV PET with Cloisite 15A in amounts of 2, 3, 4, and 5 wt %. Cloisite 10A and 30B nanocomposites were prepared at concentrations of 3 and 5 wt %. Differences between equivalent extrusion and SSP values indicate relative SSP rates.

slower than that of pure PET. Among the three nanocomposites, the SSP rate of the Cloisite 30B nanocomposite was faster than those of the Cloisite 10A and 15A nanocomposites, which were similar. Increased amounts of Cloisite 15A clay in the PET nanocomposite did not affect the SSP rate except at the highest (5 wt %) concentration.

The SSP rates of nanocomposites prepared from 0.74 IV PET were very slow; therefore, SSP temperatures were increased from 220°C to 230°C, for those prepared from lower IV PET. After 17 h of SSP at 230°C, nanocomposites prepared from PET with initial IV values of 0.63 and 0.48 dL/g, showed trends similar to those observed for the previously described samples. SSP rates of Cloisite 30B nanocomposites were faster than recorded for those containing Cloisite 10A and Cloisite 15A clays.

As described above, the organically modified nanocomposites underwent SSP at slower rates than unmodified PET. Among possible causes for the slower nanocomposite rates are the clay particle platelet structures, with length to thickness characteristics that increase the diffusion path lengths for removal of volatile polymerization products. Ethylene glycol (EG) is a major gaseous product of SSP reactions and the rates of these reactions depend on the rates of ethylene glycol diffusion from the PET matrix. These rates are slow, even from unmodified PET. For example, an EG diffusion coefficient of 1.9×10^{-6} cm²/sec has been calculated for 1 mm PET pellets at a SSP temperature of 220°C.^{40,41}

An additional reason for these slower SSP rates is an increase in PET nanocomposite crystallinity induced by the presence of clay. Clay particles can act as nuclei (enhancing rates of crystallization as shown in Figure 6) so that the addition of clay can increase the crystallinity of the nanocomposite. An increase in nanocomposite crystallinity also could increase the path length tortuosity of gaseous byproducts, causing corresponding decreases of their diffusion rates. Increased levels of crystallinity

also require higher activation energies for SSP reactions to occur. This would also decrease nanocomposite SSP rates.

Other researchers have reported increased rates of SSP for their montmorillonite (MMT) nanocomposites. Papaspyrides et al.⁴² reported significant acceleration of the SSP process for their poly(hexamethylenedipamide; PA 6.6)/clay nanocomposites. They attributed the increased rates to an increased concentration of reactive end groups in the amorphous phase, chain extension by clay SiOH groups, and to thermal protection of the polyamide matrix by the nanoparticles. Yu et al.⁴³ found increased rates of SSP in a commercially prepared PET/MMT system and attributed this to the nucleation effects of MMT, which resulted in lower crystallinity, smaller crystals, and more surfaces of the crystals. They indicated that this resulted in richer amorphous regions and better diffusion of volatile by-products for higher rates of SSP.

The first of these investigations utilized a polymer other than PET. In the second case, the mode of nanocomposite preparation and nature of the MMT are not provided. Differences in SSP rates obtained in our experiments versus those of the above researchers could also result from particle sizes. The Pa 6.6/clay nanocomposite particle sizes were from 1.14–1.70 μm and those of the PET/MMT system were not specified. Nanomaterial pellets used in our SSP reactions had an average diameter of 3.0 mm. In the case of larger particle sizes, diffusion plays a more significant role in rate of SSP, which would be reduced by any impediment such as that resulting from the clay particles and polymer crystallinity.

End group concentrations, pellet sizes, and catalyst systems are all factors that can affect SSP reactions.^{44,45} The higher end group concentrations present among the nanocomposites would be expected to contribute to faster SSP rates; however, results show that overall they did not have this influence in the reactions in comparison to unmodified PET. Among the nanocomposites, however, those containing the Cloisite 30 B (with hydroxyl group modification) exhibited the most rapid SSP rates. Pellet sizes and PET catalyst systems are equivalent among these samples, because the same (0.74 dL/g IV) PET resin was used to prepare these SSP nanocomposites. These results indicate that the effects of end group concentrations on SSP rates are less important than those of platelet structure and crystallinity.

Basal spacing can be used as an indication of clay platelet separation or penetration by polymer molecules. Initial basal spacings of the organically modified clays were measured to compare values provided by the manufacturer with those obtained under our experimental conditions. The X-ray diffraction scans obtained for the three modified clays are shown in Figure 8(a). The basal spacings for Cloisite 10A are 20.5 Å, for Cloisite 15A they are 32.7 Å and for Cloisite 30B they are 19.3 Å. Corresponding values supplied by the clay manufacturer are 19.2 Å, 31.5 Å, and 18.5 Å. The measured values are about 1 Å higher than the provided values.

The three clays, used for melt intercalation with PET, were selected in order to investigate the relative effects of their organic modifiers on the resultant nanostructures in terms of their

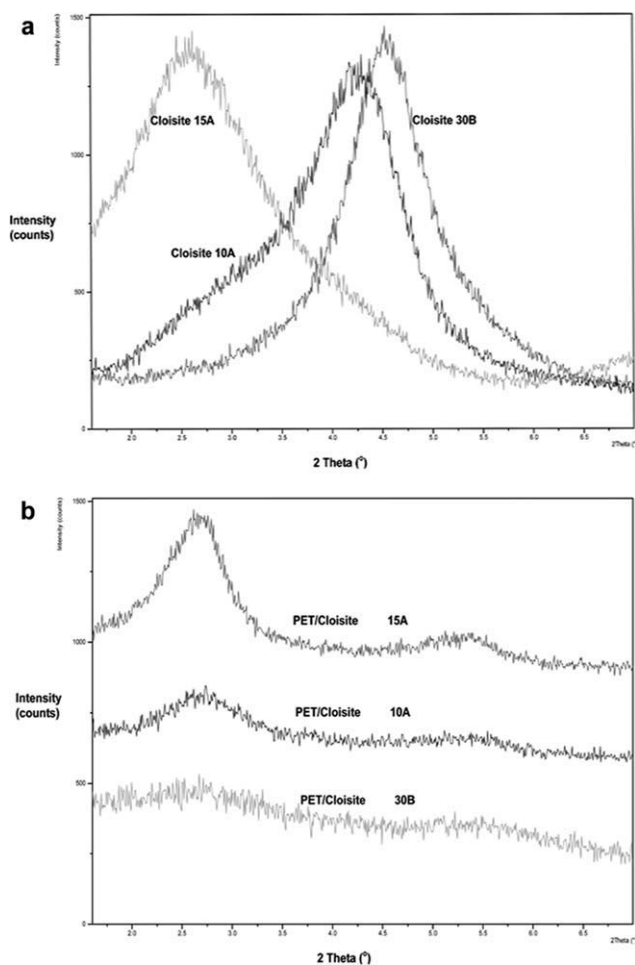


Figure 8. X-ray diffraction (XRD) spectra obtained in the 2θ range from 1.6° (55 \AA) to 7° (12.6 \AA) of (a) Cloisite 10A, 15A, and 30B clays in the absence of PET and (b) for nanocomposites prepared from 0.74 IV PET and Cloisite 10A, 15A, and 30B.

various hydrophobicities and polar interactions. Figure 8(b) shows examples of XRD peak intensities recorded for the three nanocomposites, prepared at concentrations of 3 wt %. Peak locations are similar for all three materials; however, intensity of the Cloisite 30B nanocomposite pattern is the weakest of the three samples. This indicates that Cloisite 30B may have a better affinity with the PET chains than the other modified clays. These results; however, do not indicate the presence of completely exfoliated structures, which would not show any XRD peaks. It is presumed that the 3–5 min extruder mixing time was not sufficient to permit the PET chains to fully penetrate the Cloisite 30B gallery or that the polymer size is too large for it to completely penetrate the gallery.

Cloisite 10A was expected to exhibit moderate compatibility and better hydrophobicity than Cloisite 15A, because in the case of this modifier a benzene ring structure has been substituted for the hydrogenated tallow group. The absence of strong polar groups makes any interactions between the modifier and the montmorillonite layers weaker. The intensity of the XRD peak of the Cloisite 10A nanostructure is between that of the Cloisite

15A (with almost no change) and that of Cloisite 30B (with the greatest change) meaning the affinity of Cloisite 10A is in the medium range between that of the other two materials.

The Bragg equation was used to calculate the basal spacing for each of the prepared nanocomposites. As seen in the XRD scans in Figure 8(b), the basal spacings of the Cloisite 10A and 30B nanocomposites becomes larger after extrusion, indicating that the PET is somewhat intercalated into the interlayers of these organic clays. An increase of clay amount from 3 to 5 wt % also was seen to increase the basal spacing of these nanocomposites. The basal spacing of PET/15A nanocomposite did not significantly change from that of the unblended clay. In addition, increased concentrations of 15A clay did not change the basal spacings of these nanocomposites. These results indicate that little if any intercalation occurred in nanocomposites prepared from Cloisite 15A. Nanocomposites containing 3 wt % Cloisite 10A and 30B showed respective basal spacing increases of 11.8 and 12.6 \AA in comparison to their unblended values, indicating that Cloisite 10A and 30B have some affinity with PET. These 2 results can be related to the characteristics of clays shown in Table I.

Lebaron et al.⁴⁶ reported that surface polarities of the polymer and organic clay should be matched in order for the polymer to fully wet the clay and intercalate its interlayer spaces. Polar interaction⁴⁷ is also critical for the formation of intercalation or exfoliation of nanostructure, especially when nanocomposites are prepared by a melt blending method. Unblended Cloisite 15A contains the largest initial interlayer spacing, which should allow easier intercalation of the PET molecules. There were; however, no increases in its basal spacings after extrusion. Since Cloisite 15A is strongly hydrophobic, the polarity between it and the PET was not well matched and there were no polar interactions. This caused the Cloisite 15A to be poorly dispersed in the PET matrix with no expansion of the interlayer spacing.

As previously discussed, the modifier of Cloisite 10A contains a benzene ring structure that offers some compatibility with the PET as indicated by its increased basal spacing after melt intercalation. The Cloisite 30B material possesses two hydroxyl groups in its modifier, which enables it to interact strongly with hydroxyl and carboxyl end groups of the PET molecules. This interaction promotes the intercalation of the PET molecules into the Cloisite 30B galleries. The hydrophobicity of Cloisite 30B is more similar to that of natural clay than that of Cloisite 15A. According to the above results, characteristics of the various modifiers in clay can result in different affinities with the PET molecules resulting in various nanostructures. The melt intercalation method is not sufficient to form completely exfoliated nanostructures among the evaluated modified clays. Exfoliation might be possible through melt intercalation if the modifier could be designed to give the PET molecules much better affinity with the clay, in terms of polarity, hydrophobicity, and interactivity.

To evaluate the effects of mobility of the PET chains, similar experiments were performed with lower IV PET resins. It was expected that shorter PET chains might penetrate the interlayers of the clay platelets more easily than the higher IV PET. A

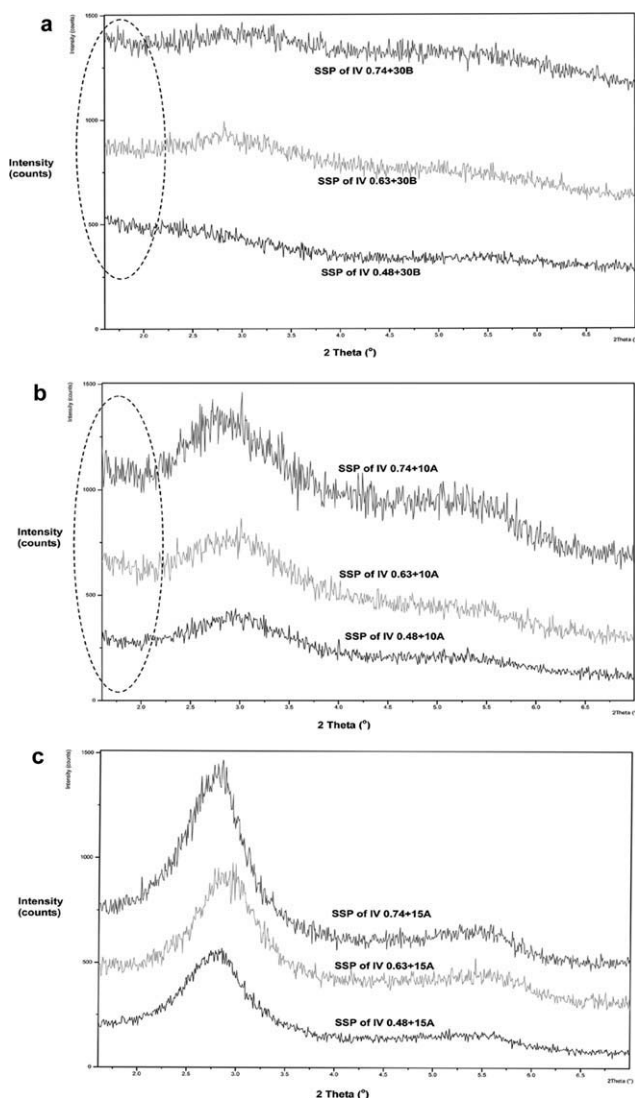


Figure 9. X-ray diffraction (XRD) spectra obtained in the 2θ range from 1.6° (55 \AA) to 7° (12.6 \AA), for nanocomposites prepared from 3 wt % of the various clays in 0.74, 0.63, and 0.48 IV PET resins. New low angle XRD peaks are present (within the dashed ellipse) after completion of the SSP reactions with (a) Cloisite 30B and with (b) Cloisite 10A. In the case of (c) Cloisite 15A, no new low angle XRD peaks are present.

comparison was made among PET resins with initial IV values of 0.48, 0.63, and 0.74 dL/g. The basal spacings of their nanocomposites; however, were not significantly changed. The nanocomposite prepared from PET with an initial IV of 0.48 dL/g, had the largest basal spacing. The differences between use of 0.48 and 0.74 dL/g PET; however, were small indicating that within this IV range the effects of molecular weight on nanostructure resulting from the melt intercalation method are not significant.

Various nanocompounds that had been prepared through melt mixing were also SSP to higher molecular weights. These SSP samples were characterized with X-ray diffraction, to evaluate effects of the additional thermal histories on their nanostructures and basal spacings. It was expected that if some of the

PET chain ends had been located in the galleries of the clay platelets through melt mixing, they might exhibit expansion as a result of SSP reactions.

XRD scans of SSP nanocomposites containing Cloisite 30B and 10A exhibited new peaks at low angles, while no changes in peak positions were present for nanocomposites containing Cloisite 15A. Figure 9(a–c) gives examples of these diffraction scans, with locations of the new peaks indicated by the dashed ellipses. (Spectra recorded for the nanocomposites before SSP did not show any new peak at low angles.) Although it is known that XRD has limitations in terms of measuring the peaks located at angles lower than 1.6° , it is apparent that the new peaks are located in this spectral region. This finding is significant, because it indicates that the basal spacings of these samples must be larger than 55 \AA . These results indicate that the basal spacings of melt extrusion nanocomposites were expanded during the SSP reaction for samples containing Cloisite 30B and 10A.

Figure 10 gives an overview of basal spacing values measured for each of the Cloisite materials before being compounded with PET, after melt blending at 3 wt %, and after SSP with each IV PET. The figure is labeled to indicate each clay and IV. In the sets of two bars for each IV PET, the first bar represents before and the second bar illustrates after SSP. These results indicate that in most cases the basal spacings, represented by the primary XRD peaks, are reduced after SSP. The nanocomposite prepared from 0.48 IV PET and 3 wt % Cloisite 30B is the only sample to clearly show an increase in basal spacing as a result of SSP.

X-ray diffraction scans of Cloisite 30B and 10A [Figure 9(a,b)] indicate that the SSP reaction had positive effects on basal spacing expansion in the PET nanocomposites. This expansion,

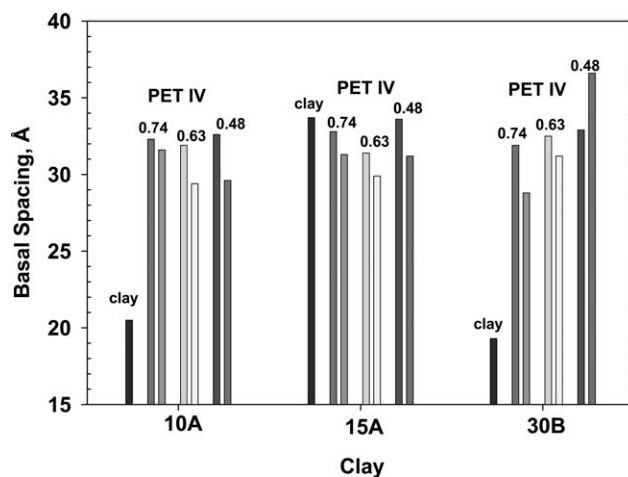


Figure 10. Basal spacing values are given in an overview that includes each of the Cloisite materials (10A, 15A, and 30B) before being compounded with PET, after melt intercalation into 3 wt % nanocomposites, and after SSP with 0.48, 0.63, and 0.74 dL/g IV PET resins. In the paired data sets prepared from each PET IV, the first bar represents the extruded nanocomposite before SSP and the second bar after SSP for 15 h at 220 or 230°C .

however, did not occur in all the clay platelets, as can be observed in the overview given in Figure 10. Most of the basal spacings have decreased slightly as a result of the SSP reaction. Peak movements to higher angles, which mean basal spacings are reduced, may be related to thermal degradation during the SSP reactions. Nanocomposites were heated for 15 h at 220 or 230°C during SSP, which could cause degradation of the organic clay modifier. This will be evaluated more thoroughly in an additional study utilizing *in situ* polymerization.²⁰ In the case of *in situ* polymerization, nanocomposites are exposed to higher levels of heat during melt polymerization. The small peak present at 5.6° (15–16 Å) indicates that some portion of the modified clay was changed to natural MMT peak basal spacing (~12 Å). It is also important to note that basal spacing values shown in Figure 10 do not take into consideration the presence of new peaks indicated by the dashed ellipses given in Figure 9(a,b). They also fail to indicate the substantial reductions in peak sizes exhibited most strongly by the XRD scans of Cloisite 30B nanocomposites shown in Figure 9(a).

Figure 9(a) shows that the XRD peak shape of the SSP nanocomposite prepared from 0.48 IV PET and Cloisite 30B was different from that of other XRD shapes recorded for SSP nanocomposites. In this case, the peak intensity increases continuously from 4.5° to 1.6°. This material was the most effective for obtaining improved nanostructure through use of a melt intercalation method. These results indicate that of the evaluated clays, the Cloisite 30B material has the best affinity with PET molecules and that use of lower IV PET can result in improved nanostructure. Although melt blending has been able to achieve some changes in nanostructure, indicating that intercalation has occurred, the existence of XRD peaks indicate that the clay structure has not been completely exfoliated. For this reason no electron microscopy or TEM analyses were performed on these nanocomposites.

CONCLUSIONS

Three molecular weights of PET were separately compounded with each of three organo-montmorillonite clays at 275°C using a twin screw extruder. Selected samples were also solid state polymerized to increase their molecular weights and basal spacings. Mobility effects of the PET chains and affinity effects of the clay modifiers were monitored in order to characterize the effects of these variables on resultant nanostructures. Results of these evaluations indicate the following:

- Cloisite 30B clay has the strongest affinity with PET molecules as a result of the two hydroxyl groups in its modifier. These enable it to interact with the hydroxyl and carboxyl end groups of the PET molecules resulting in its intercalation into the Cloisite 30B galleries. Cloisite 10A also shows some intercalation; however, Cloisite 15A shows no affinity with PET.
- The greater mobility of lower IV PET results in its improved penetration of the clay galleries, especially as a result of SSP of nanocomposites containing Cloisite 30B.
- After solid state polymerization, nanocomposites containing Cloisite 10A and Cloisite 30B show additional low angle XRD peaks, illustrating that some parts of clay have larger

basal spacings than 55 Å, although samples prepared by the melt blending method do not show completely exfoliated nanostructures.

- Addition of clay results in molecular weight reduction of the PET nanocomposites, indicating that clay modifiers can affect degradation rates of the nanocomposites.
- Thermal stability experiments show that thermal degradation rates of the nanocomposite are faster than that of unblended PET.
- End group analysis shows that hydrolysis is the major cause of molecular weight reductions during compounding at 275°C.
- The SSP rates of the nanocomposites are slower than that of PET, because of the platelet structures of clay particles, which impede the diffusion of volatile gasses.
- Crystallization rates, when heated from room temperature and when cooled from melt state, are accelerated due to the addition of clay particles.

ACKNOWLEDGMENTS

The authors thank the members of the PET Industrial Consortium who have supported this research at the Polymer Institute of the University of Toledo.

REFERENCES

1. Jabarin, S. A. *Polymeric Materials Encyclopedia*; CRC: Boca Raton, FL, **1996**; Vol. 8, pp 6078, 6091.
2. Ke, Y. C.; Yang, Z. B.; Zhu, C. F. *J. Appl. Polym. Sci.* **2002**, *85*, 2677.
3. Carrado, K. A.; Shonaike, G. O.; Advani, S. G. *Advanced Polymeric Materials*; CRC: Boca Raton, FL, **2003**; Chapter 10.
4. Ray, S. S.; Okamoto, M. *Prog. Polym. Sci.* **2003**, *28*, 1539.
5. Wang, Z.; Massam, J.; Pinnavaia, T. J. *Polymer-Clay Nanocomposites*; Pinnavaia, T. J., Beall, G. W., Eds.; John Wiley & Sons Ltd: New York, **2000**; Chapter 7.
6. Hay, J. N.; Shaw, S. J. *A Review of Nanocomposites*. www.azom.com **2000**.
7. Li, X.; Kang, T. K.; Cho, W. J.; Lee, J. K.; Ha, C. S. *Macromol. Rapid Commun.* **2001**, *22*, 1306.
8. Chang, J. H.; Kim, S. J.; Joo, Y. L.; Im, S. S. *Polymer* **2004**, *45*, 919.
9. Matayabas Jr., J. C.; Turner, S. R. *Polymer-Clay Nanocomposites*; Pinnavaia, T. J., Beall, G. W., Eds.; John Wiley & Sons Ltd: New York, **2000**; Chapter 11.
10. Alexandre, M.; Dubois, P. *Mater. Sci. Eng.* **2000**, *28*, 1.
11. Blumstein, A. *J. Polym. Sci. A* **1965**, *3*, 2665.
12. Krishnamoorti, R.; Vaia, R. A.; Giannelis, E. P. *Chem. Mater.* **1996**, *8*, 1728.
13. Gilman, J. W.; Jackson, C. L.; Morgan, A. B.; Harris, R.; Manias, E.; Giannelis, E. P.; Wuthenow, M.; Hilton, D.; Phillips, S. H. *Chem. Mater.* **2000**, *12*, 1866.
14. Sposito, G.; Skipper, N. T.; Sutton, R.; Park, S. H.; Soper, A. K.; Greathouse, J. A. *Proc. Natl. Acad. Sci.* **1999**, *96*, 3358.

15. Xie, W.; Gao, Z.; Pan, W. P.; Hunter, D.; Singh, A.; Vaia, R. *Chem. Mater.* **2001**, *13*, 2979.
16. Barber, G. D.; Bellman, S. P.; Moore, R. B. *ANTEC* **2003**, 1369.
17. Barber, G. D.; Calhoun, B. H.; Moore, R. B. *Polymer* **2005**, *46*, 6706.
18. Davis, C. H.; Mathias, L. J.; Gilman, J. W.; Schiraldi, D. A.; Shields, J. R.; Trulove, P.; Sutto, T. E.; Delong, H. C. *J. Polym. Sci. Part B: Polym. Phys.* **2002**, *40*, 2661.
19. Sanchez-Solis, A.; Garcia-Rejon, A.; Manero, O. *Macromol. Symp.* **2003**, *192*, 281.
20. Nanocomposite Development with Organically Modified Clay through *In Situ* Polymerization; to be submitted to *J. Appl. Polym. Sci. in* **2012**.
21. Southern Clay Products, Inc. webpage, <http://www.nanoclay.com/>
22. Zhang, H.; Rankin, A.; Ward, M. *Polymer* **1996**, *37*, 1079.
23. Al-Abdul Razzak, S.; Lofgren, E. A.; Jabarin, S. A. *Polym. Int.* **2002**, *51*, 174.
24. Kim, T. Y.; Lofgren, E. A.; Jabarin, S. A. *J. Appl. Polym. Sci.* **2003**, *89*, 197.
25. Jabarin, S.; Lofgren, E. *J. Appl. Polym. Sci.* **1986**, *32*, 5315.
26. Rabeck, J. F. *Experimental Methods in Polymer Chemistry*; Wiley: New York, **1980**; Chapter 28.
27. Xie, W.; Gao, Z.; Liu, K.; Pan, W. P.; Vaia, R.; Hunter, D.; Singh, A. *Thermochimica Acta* **2001**, *367*, 339.
28. Krishnamoorti, R.; Silva, A. S. In *Polymer-Clay Nanocomposites*; Pinnavaia, T. J., Beall, G. W., Eds.; John Wiley & Sons Ltd: New York, **2000**; Chapter 15.
29. Yuki, K. *Saturated Polyester Resin Handbook*; Nikkan Kougyosha: Tokyo, **1989**; Chapter 3.
30. Al-Abdul Razzak, S.; Jabarin, S. A. *Polym. Int.* **2002**, *51*, 164.
31. Villain, F.; Coudane, J.; Vert, M. *Polym. Degrad. Stab.* **1995**, *49*, 393.
32. Campanelli, J. R.; Cooper, D. G.; Kamal, M. R. *J. Appl. Polym. Sci.* **1994**, *53*, 985.
33. Xu, X.; Ding, Y.; Quian, Z.; Wang, F.; Wen, B.; Zhou, H. *Polym. Degrad. Stab.* **2009**, *94*, 113.
34. Goodings, E. P. *Society of Chemical Industry Monograph No* **1961**, *13*, 211.
35. Ritchie, P. D. *Society of Chemical Industry Monograph No*, **1961**, *13*, 107.
36. Marshall, I.; Todd, A. *J. Chem. Soc. Faraday Trans.* **1953**, *49*, 67.
37. McMahon, W.; Birdsall, H. A.; Johnson, G. R.; Camilli, C. T. *J. Chem. Eng. Data* **1959**, *4*, 57.
38. Yoda, K.; Tsuboi, A.; Wada, M.; Yamadera, R. *J. Appl. Polym. Sci.* **1970**, *14*, 2357.
39. Ebengou, R. H. *J. Polym. Sci. Part B: Polym. Phys.* **1997**, *35*, 1333.
40. Kesaboina, S. R.; Lofgren, E. A.; Jabarin, S. A. *Polym. Eng. Sci.* **2012**.
41. Mallon, F. K.; Ray, W. H. *J. Appl. Polym. Sci.* **1998**, *69*, 1233.
42. Boussia, A. C.; Konstantakopoulou, M. O.; Vouyiouka, S. N.; Papaspyrides, C. D. *Macromol. Mater. Eng.* **2011**, *296*, 168.
43. Yu, H.; Han, K.; Yu, M. *J. Appl. Polym. Sci.* **2004**, *94*, 971.
44. Huang, B.; Walsh, J. J. *Polymer* **1998**, *39*, 6991.
45. Ravindranath, K.; Mashelkar, R. *J. Appl. Polym. Sci.* **1990**, *39*, 1325.
46. Lebaron, P. C.; Wang, Z.; Pinnavaia, T. *J. Appl. Clay Sci.* **1999**, *15*, 11.
47. Yoon, J. T.; Jo, W. H.; Lee, M. S.; Ko, M. B. *Polymer* **2001**, *42*, 329.